EARTHQUAKE ENGINEERING AND STRUCTURAL DYNAMICS, VOL. 25, 529–545 (1996)

# TIME-DOMAIN ANALYSIS OF LINEAR HYSTERETIC DAMPING

JOSÉ A. INAUDI*
*University of California at Berkeley, EERC, 1301 South 46th St., Richmond, CA 94804, U.S.A.*

AND

NICOS MAKRIS†
*Department of Civil Engineering and Geological Sciences, University of Notre Dame, Notre Dame, IN 46556, U.S.A.*

## SUMMARY

Two linear-hysteretic-damping models that provide energy dissipation independent of the deformation frequency, are studied in this paper: a hysteretic Kelvin element and a hysteretic Maxwell element. Both models use the Hilbert transform and yield integro–differential equations for the equations of motion of structures when real-valued signals are utilized in the formulation. It is shown that the use of analytic (complex-valued) signals allows the transformation of these integro–differential equations into differential equations with analytic input signals and complex-valued coefficients. These differential equations show both stable and unstable poles. A technique for the solution of these differential equations is presented; it consists of a conventional modal decomposition of the state-space equations and the integration of the differential equations forward in time for the modal co-ordinates associated with stable poles, and backwards in time for the modal co-ordinates associated with unstable poles. Some numerical examples are presented to illustrate the characteristics of the models and the proposed analysis technique.

KEY WORDS: structural damping; energy dissipation; Hilbert transform; analytic signals

## 1. INTRODUCTION

Dampers for reducing vibrations in structures utilize different energy dissipation mechanisms such as friction, phase-transformations, plasticity and viscosity. Materials such as asphalt, acrylic polymers, and rubber exhibit significant energy dissipation when deformed cyclically with minor dependence of the energy dissipation on the deformation frequency and with quadratic dependence of the energy dissipation per cycle on the deformation amplitude. Accordingly, different viscoelastic models have been proposed to approximate the frequency dependence of mechanical properties.[1–4]

The idealization of force-deformation relations exhibiting rate-independent hysteresis is referred to as hysteretic behaviour. According to Bishop,[5] linear models for hysteretic damping were proposed prior to 1937. Denominations such as linear hysteretic damping, structural damping, or complex-valued stiffness, have been used in the literature to refer to a linear model of damping in which the energy loss per cycle is independent of the deformation frequency. Interesting discussions on this model can be found in the literature.[5–10]

In addition to the materials mentioned above, some non-linear dampers and semi-active damping devices show hysteretic behaviour with quadratic dependence of cyclic dissipation on deformation amplitude and no dependence on the deformation frequency.[11–13] In these cases, a linear model may be preferred over a non-linear model because of its simpler mathematical tractability. Fourier analysis, for example, is useful for analyzing linear structural models but is of little use for analysis of non-linear models, because the

*Assistant Research Engineer
†Assistant Professor. Member ASCE

CCC 0098–8847/96/060529–17

*Received 23 May 1995*
*Revised 26 September 1995*

superposition principle does not hold in non-linear systems. For this reason, linear constitutive models that can capture the hysteretic nature of materials are valuable, even when these models may yield non-causal (anticipatory) input–output operators which are not physically sound. In fact, linearization techniques based on the concept of linear hysteretic damping have proven very accurate and practical for the design of structures with a class of non-linear dampers.[14]

Any linear time-invariant constitutive relationship can be expressed in the frequency domain as

$$F(\mathrm{j}\bar{\omega}) = (G_s(\bar{\omega}) + \mathrm{j}G_l(\bar{\omega}))\Delta(\mathrm{j}\bar{\omega}) \tag{1}$$

where $F(\mathrm{j}\bar{\omega})$ is the Fourier transform of the real-valued force signal $f(t)$, $\Delta(\mathrm{j}\bar{\omega})$ the Fourier transform of the real-valued deformation signal $\Delta(t)$, $G_s(\bar{\omega})$ the real-valued storage modulus, $G_l(\bar{\omega})$ the real-valued loss modulus and $\mathrm{j} = \sqrt{-1}$.

The energy dissipation in a cycle of steady-state sinusoidal deformation of frequency $\bar{\omega}$ and amplitude $\Delta_0$ is

$$W_D = \pi |G_l(\bar{\omega})| \Delta_0^2 \tag{2}$$

In this paper we deal with two linear models that can be used to represent hysteretic materials. These models show constant storage and loss moduli,

$$G_s(\bar{\omega}) = k, \quad \bar{\omega} \neq 0 \tag{3}$$

$$G_l(\bar{\omega}) = \eta k \operatorname{sgn}(\bar{\omega}) \tag{4}$$

where $k$ is the frequency-independent stiffness parameter, $\eta$ the frequency-independent loss factor (ratio of the loss and storage moduli), and $\operatorname{sgn}(x) = 1$ if $x > 0$, $\operatorname{sgn}(x) = 0$ if $x = 0$, and $\operatorname{sgn}(x) = -1$ if $x < 0$.

Time-domain models of hysteretic damping are investigated in this work. In particular, the hysteretic Kelvin and Maxwell elements are studied using efficient time-domain tools such as differential equations with complex-valued coefficients and analytic signals. As an alternative approach, formulations using real-valued signals and integro–differential equations are presented.

## 2. MATHEMATICAL PRELIMINARIES

Before describing the models studied, we review the definition and relevant properties of the Hilbert transform and of analytic signals which are utilized extensively herein.

### *2.1. The Hilbert transform*

The functions $y(t)$ and $\hat{y}(t)$ are called a Hilbert transform pair if, for almost all $t$,

$$\hat{y} = H[y(t)] = \lim_{a\to\infty} \mathrm{P} \int_{-a}^{a} \frac{-y(\tau)}{\pi(t-\tau)}\,\mathrm{d}\tau \tag{5}$$

$$y(t) = H^{-1}[\hat{y}(t)] = \lim_{a\to\infty} \mathrm{P} \int_{-a}^{a} \frac{\hat{y}(\tau)}{\pi(t-\tau)}\,\mathrm{d}\tau \tag{6}$$

where

$$\mathrm{P}\int_{-\infty}^{\infty} \frac{f(\tau)}{t-\tau}\,\mathrm{d}\tau = \lim_{\varepsilon\to 0^+} \left[ \int_{t+\varepsilon}^{\infty} \frac{y(\tau)}{t-\tau}\,\mathrm{d}\tau + \int_{-\infty}^{t-\varepsilon} \frac{y(\tau)}{t-\tau}\,\mathrm{d}\tau \right] \tag{7}$$

is called the Cauchy principal value around $\tau = t$ of the integral. We say that $\hat{y}(t)$ is the Hilbert transform of $y(t)$, and we write $\hat{y}(t) = H[y(t)]$.[15]

As shown in equation (5), the Hilbert transform of a signal $y(t)$ is a linear operator defined by the convolution of $y(t)$ and $-1/(\pi t)$. Equation (5) also shows that this operator is non-causal, because in order to compute $\hat{y}(t)$, the function $y\tau$ is required for $-\infty < \tau < \infty$; that is, the future of the signal is required to compute the Hilbert transform of the signal at present time.

The Hilbert transform has a similarity property under time scaling; this means that if $\hat{y}(t)$ is the Hilbert transform of $y(t)$, $\hat{y}(\alpha t)$ is the Hilbert transform of $y(\alpha t)$ for any $\alpha > 0$.[16]

Consider the signal $y(t) = \sin \bar{\omega} t$ with $\bar{\omega} \neq 0$; its Hilbert transform is

$$H[\sin \bar{\omega} t] = \int_{-\infty}^{\infty} \frac{-\sin \bar{\omega} \tau}{\pi(t-\tau)} \, d\tau = \cos \bar{\omega} t \, \mathrm{sgn}(\bar{\omega}) \tag{8}$$

Similarly,

$$H[\cos \bar{\omega} t] = -\sin |\bar{\omega}| t \tag{9}$$

As shown in equations (8) and (9), the Hilbert transform does not change the amplitude of a sine or cosine signal and only produces a phase shift of $+\pi/2$ or $-\pi/2$ radians in these signals.

This transform is a useful tool for linear models of hysteretic behavior.[17] A mechanical model is said to be hysteretic or rate-independent when

$$f(\alpha t) = E[\Delta(\alpha t)], \quad \alpha > 0 \tag{10}$$

where $f(t)$ is the $E[\Delta(t)]$ element force, $\Delta(t)$ the element deformation $E[\Delta(t)]$ the operator relating deformation to force, and $\alpha$ a positive scalar. As indicated in equation (10), a hysteretic model has a similarity property which is also a property of the Hilbert transform.

From equation (5) we can prove that the Hilbert transform of a constant signal is zero. This implies that equation (6) recovers the whole frequency content of the original signal except for the zero-frequency component which is zero in $\hat{y}(t)$. Therefore,

$$H[H[y(t)]] = -y(t) \tag{11}$$

only if $y(t)$ has no zero-frequency component.

The Hilbert transform commutes with other linear operators such as differentiation; thus,

$$H\left[\frac{dy(t)}{dt}\right] = \frac{d}{dt} H[y(t)] \tag{12}$$

Equation (11) holds for all signals with no zero-frequency components. A time-derivative signal $\dot{y}(t) = dy(t)/dt$ has no zero-frequency component; therefore, we can write

$$H[H[\dot{y}(t)]] = -\dot{y}(t) \tag{13}$$

Finally, let us analyze the Hilbert transform in the frequency domain. Recalling that Hilbert transform is the following convolution

$$\hat{y}(t) = y(t) * \left(-\frac{1}{\pi t}\right) \tag{14}$$

and that the Fourier transform (FT) of $(-1/(\pi t))$ is

$$\mathrm{FT}\left[-\frac{1}{\pi t}\right] = j \, \mathrm{sgn}(\bar{\omega}) \tag{15}$$

we obtain

$$\hat{Y}(j\bar{\omega}) = j \, \mathrm{sgn}(\bar{\omega}) \, Y(j\bar{\omega}) \tag{16}$$

As indicated in this equation, the Hilbert transform maintains the magnitude of the signal at all frequencies except for $\bar{\omega} = 0$ which is filtered completely from the original signal.

Figure 1 shows a decaying exponential signal $y(t) = e^{-\omega\zeta t} \cos \omega t$ and its corresponding Hilbert transform. The following parameters were selected: $\omega = 4\pi$ rad/s and $\zeta = 0{\cdot}10$. As the figure illustrates, $\hat{y}(t)$ anticipates $y(t)$. We see a phase change in $\hat{y}(t)$ that reminds us the time-derivative of $y(t)$. However, had we chosen a different frequency $\omega$, the Hilbert transform of that signal, unlike time differentiation, would have not changed in amplitude because of the similarity property of the Hilbert transform.

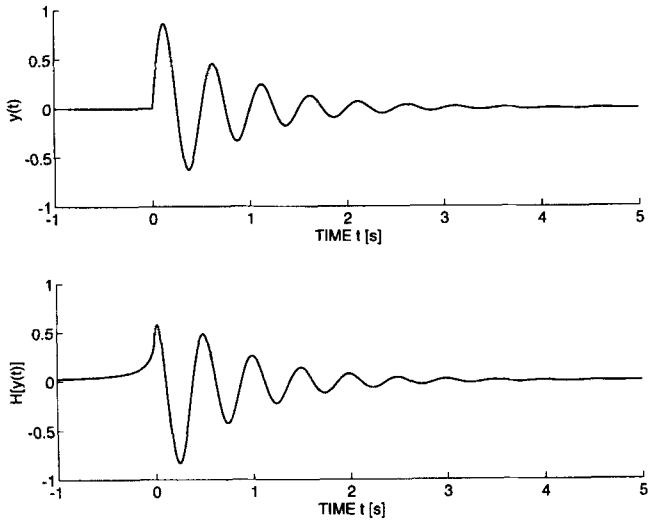


Figure 1. A signal $y(t)$1 and its Hilbert transform $H[y(t)]$

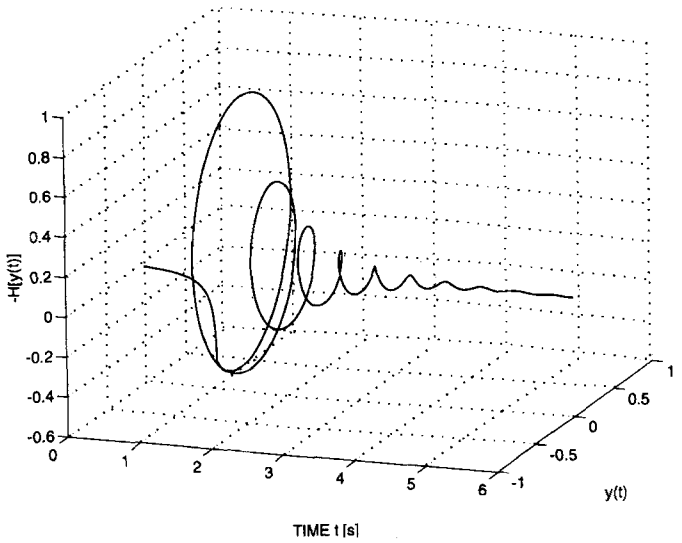


Figure 2. An analytic signal $y_a(t) = y(t) - jH[y(t)]$

## 2.2. *Analytic signals*

An analytic signal $y_a(t)$ is the complex-valued signal defined as

$$y_a(t) = y(t) - jH[y(t)] = y(t) + \frac{j}{\pi}\int_{-\infty}^{\infty} \frac{y(\tau)}{t-\tau}\,d\tau \tag{17}$$

where the real-valued functions $y(t)$ and $-H[y(t)]$, real and imaginary part of $y_a(t)$, are a Hilbert transform pair.[16] Figure 2 shows in a three-dimensional plot, the analytic signal $y_a(t)$ created using the signals $y(t)$ and $H[y(t)]$ described in Figure 1. The imaginary component of the signal is displayed in the vertical axis; the real part of the signal and time are shown in the horizontal axes.

Let us analyze the frequency content of an analytic signal. Taking Fourier transform of equation (17) and using equation (16), we obtain

$$Y_a(j\bar{\omega}) = Y(j\bar{\omega})(1 + \mathrm{sgn}(\bar{\omega})) \tag{18}$$

where $Y_a(j\bar{\omega}) =$ Fourier transform of $y_a(t)$. Because $y(t)$ is real valued, $\mathrm{Re}[Y(j\bar{\omega})] = \mathrm{Re}[Y(-j\bar{\omega})]$ and $\mathrm{Im}[Y(j\bar{\omega})] = -\mathrm{Im}[Y(-j\bar{\omega})]$; therefore,

$$Y_a(j\bar{\omega}) = 0, \quad \bar{\omega} < 0 \tag{19}$$

This shows that an analytic signal has no negative-frequency components.

## 3. HYSTERETIC LINEAR DASHPOT

In this paper, we use the concept of hysteretic linear dashpot. Used in parallel and series connections with a conventional linear spring, this model allows us to create hysteretic Kelvin and Maxwell elements, respectively.

A linear hysteretic dashpot is a damping model that satisfies[18]

$$f(t) = S_h \hat{\Delta}(t) = -\frac{S_h}{\pi} \int_{-\infty}^{\infty} \frac{\Delta(\tau)}{t - \tau} \, d\tau \tag{20}$$

where $f(t)$ is the force in the element, $S_h$ the parameter with units of stiffness characterizing the dashpot and $\hat{\Delta}(t)$ the Hilbert transform of the deformation signal $\Delta(t)$. Both $\hat{\Delta}(t)$ and $S_h$ are real-valued; therefore, this model yields a real-valued force signal.

Applying Fourier transform to equation (20), we obtain

$$F(j\bar{\omega}) = j S_h \mathrm{sgn}(\bar{\omega}) \Delta(j\bar{\omega}) \tag{21}$$

which shows that the hysteretic linear dashpot is purely dissipative because the storage modulus of this element vanishes for all $\bar{\omega}$. From equations (2) and (21) we see that

$$W_D = \pi S_h \Delta_0^2 |\mathrm{sgn}(\bar{\omega})| \tag{22}$$

which confirms the fact that this model dissipates the same amount of energy in a harmonic deformation cycle of amplitude $\Delta_0$ for any deformation frequency $\bar{\omega} \neq 0$.

Figure 3 shows a sinusoidal deformation signal, $y(t) = \Delta_0 \sin \bar{\omega} t \, U(t)$ (in thin line), and the corresponding damper force (thick line) $f(t) = S_h \Delta_0 H[\sin(\bar{\omega} t) U(t)]$ where $U(t)$ is the Heaviside function; $U(t) = 0$ if $t < 0$

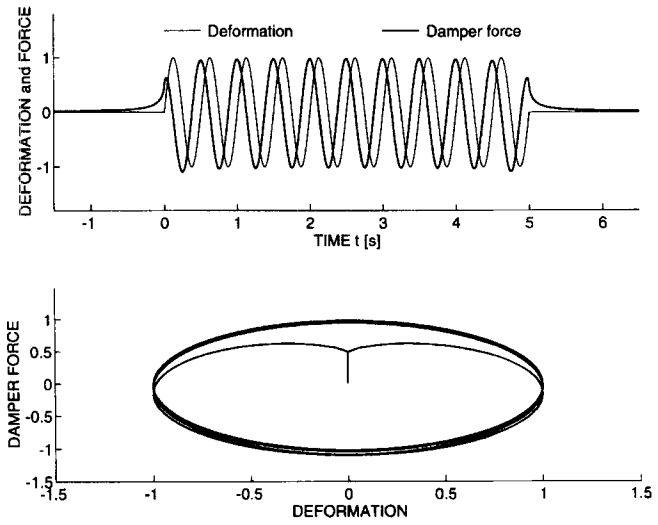


Figure 3. The force–deformation relation of a linear hysteretic damper

and $U(t) = 1$ if $t \geqslant 0$. For convenience, the deformation and damper force signals have been normalized as follows $\Delta(t)/\Delta_0, f(t)/(\Delta_0 S_h)$; $\bar{\omega}$ was taken as $4\pi$ rad/s. As shown in the figure, there is an anticipatory transient phase and steady-state phase during which the force is a cosine function (indicating a phase advance of $\pi/2$ rad with respect to the deformation signal). The figure also shows the hysteresis loops of the model which do not depend on $\bar{\omega}$.

## 4. HYSTERETIC KELVIN ELEMENT

### *4.1. Hysteretic Kelvin model using real-valued signals*

This model has been used extensively in the literature in the context of harmonic excitation[19-21] and is referred to as structural damping, complex-stiffness model, or linear hysteretic element. The model consists of a conventional linear spring in parallel with a linear hysteretic dashpot. Accordingly, the force in the model can be expressed as the sum of the forces in the spring and that in the hysteretic damper

$$f(t) = k\,\Delta(t) + S_h H[\Delta(t)] \tag{23}$$

where $k$ and $S_h$ are constants with units of stiffness.

The model has been usually presented in the frequency domain

$$F(j\bar{\omega}) = k(1 + j\eta \operatorname{sgn}(\bar{\omega}))\Delta(j\bar{\omega}) \tag{24}$$

where the loss factor $\eta$ is

$$\eta = \frac{S_h}{k} \tag{25}$$

As indicated in equation (24), this model shows constant storage and loss moduli. It is however, not able to represent residual deformation, because upon removal of the load, the element will restore without permanent deformation. This model will exhibit a restoring force or a sustained constant deformation because the storage modulus of this element at $\bar{\omega} = 0$ is not zero; in fact $G_s(0) = k$.

When this model is included in the equations of motion of structures, integro–differential equations result. These equations can be solved using fast Fourier transform (FFT) or using series of differential equations in the time domain.[17] In this paper, we propose an alternative solution technique utilizing analytic signals.

### *4.2. Hysteretic Kelvin model using analytic signals*

Although the hysteretic Kelvin model can be formulated using real-valued signals leading to integro–differential equations of motion of structures, we will prove that if we use analytic signals we can transform these integral operators into differential operators on analytic signals. This is a consequence of the commutative property of the Hilbert transform with time differentiation (see equation (12)).

Consider the model described by equation (23). Applying the Hilbert transform to this equation, we obtain

$$H[f(t)] = kH[\Delta(t)] - S_h\,\Delta(t) \tag{26}$$

where we have used the fact that $H[H[\Delta(t)]] = -\Delta(t)$. Multiplying equation (26) by $-j$ and summing the result to equation (23), we obtain the following analytic signal

$$f_a(t) = f(t) - jH[f(t)] = k\,\Delta_a(t) + S_h H[\hat{\Delta}] + jS_h\,\Delta(t)$$

which can be written as

$$f_a(t) = (k + jS_h)\Delta_a(t) \tag{28}$$

where $\Delta_a(t) = \Delta(t) - jH[\Delta(t)]$. We see that the integral operator in equation (23) on real-valued signals has been transformed into an algebraic equation relating analytic (complex-valued) signals. Using this mathematical artifice, we can attempt to solve linear models including hysteretic Kelvin elements using differential equations instead of integro–differential equations.

It is important to note that only $f(t)$, the real part of $f_a(t)$, has physical meaning; the imaginary part of $f_a(t)$ does not have a physical significance but permits the conversion of the integral equations into an algebraic relation between analytic signals.

Consider a single-degree-of-freedom (SDOF) structure with mass $m$ and linear hysteretic damping modelled as

$$m\ddot{y}(t) + ky(t) + S_h H[y(t)] = w(t) \tag{29}$$

where all signals and parameters are real-valued. Multiplying the Hilbert transform of this equation by $-j$ and summing the result to equation (29), we obtain

$$m\ddot{y}_a(t) + (k + jS_h)\, y_a(t) = w_a(t) \tag{30}$$

which is an ordinary differential equation on analytic signals. Initial conditions cannot be specified for this system because the system is non-causal.[7] In the case of finite-duration excitation signals $w(t)$, we can take

$$y(-\infty) = 0, \qquad y(\infty) = 0 \tag{31}$$

because the oscillator is stable.

Equation (30) has been utilized extensively in the context of harmonic excitation. It has been said that this equation is meaningful for excitation signals of the form $e^{j\bar{\omega}t}$. This is in fact correct because

$$e^{j\bar{\omega}t} = \cos\bar{\omega}t + j\sin\bar{\omega}t = \cos\bar{\omega}t - jH[\cos\bar{\omega}t] \tag{32}$$

which shows that the assumed excitation signal is indeed, an analytic signal. It has been argued that this equation cannot be used for arbitrary excitation signals.[19] However, provided the excitation is an analytic signal, equation (30) is a correct model for SDOF structures with hysteretic damping and its solution can be found using techniques of ordinary differential equations as we demonstrate in the sequel.

Let us use a state-space formulation to find the response of the system defined in equation (29)

$$\dot{\mathbf{x}}_a(t) = \mathbf{A}\mathbf{x}_a(t) + \mathbf{B}w_a(t) \tag{33}$$

where

$$\mathbf{x}_a(t) = \begin{bmatrix} y_a(t) \\ \dot{y}_a(t) \end{bmatrix}, \qquad \mathbf{A} = \begin{bmatrix} 0 & 1 \\ -\omega^2(1+\eta j) & 0 \end{bmatrix}, \qquad \mathbf{B} = \begin{bmatrix} 0 \\ \dfrac{1}{m} \end{bmatrix}, \qquad \omega = \sqrt{\frac{k}{m}}, \qquad \eta = \frac{S_h}{k} \tag{34}$$

and let us construct the solution of this differential equation.

The characteristic equation for this system (determinant of $s\mathbf{I} - \mathbf{A}$) is

$$s^2 + \omega^2(1 + \eta j) = 0 \tag{35}$$

whose roots (eigenvalues of $\mathbf{A}$) are

$$s_1 = -a + bj, \qquad s_2 = a - bj \tag{36}$$

where $a$ and $b$ are positive real numbers

$$a = \frac{\omega}{\sqrt{2}}\sqrt{\sqrt{1+\eta^2} - 1}, \qquad b = \frac{\omega^2\eta}{2a} \tag{37}$$

From equation (35) we note that the poles have radial symmetry with respect to the origin in the complex plane. This can be explained mathematically as follows. From equation (34)

$$\text{trace}(\mathbf{A}) = 0 \tag{38}$$

and from linear algebra we know that

$$\text{trace}(\mathbf{A}) = s_1 + s_2 \tag{39}$$

Therefore, $s_1 = -s_2$, which implies radial symmetry of the poles in the complex plane. This also implies that one pole, $s_1$, is stable and the other, $s_2$, is unstable. Attempting a standard technique for the solution of this linear system such as the discrete-time implementation of the convolution integral

$$\mathbf{x}_a(t) = \int_{-\infty}^{t} e^{\mathbf{A}(t-\tau)} \mathbf{B}\, w_a(\tau)\, d\tau \tag{40}$$

will not result in a successful solution because the unstable pole $s_2$ will generate unbounded growth of the impulse response function $e^{\mathbf{A}t}\mathbf{B}$ of this system.

Let us use the eigenvectors of $\mathbf{A}$ to uncouple the dynamics of the two modes of the system and let us reverse the time in the modal co-ordinate of the unstable mode so that stable differential equations are obtained for both modes. Defining the analytic modal coordinates $q_1(t)$ and $q_2(t)$ we can write

$$\mathbf{x}_a(t) = \mathbf{\Phi} \begin{bmatrix} q_1(t) \\ q_2(t) \end{bmatrix} \tag{41}$$

where $\mathbf{\Phi}$ is matrix of eigenvectors

$$\mathbf{\Phi} = \begin{bmatrix} 1 & 1 \\ s_1 & s_2 \end{bmatrix} \tag{42}$$

Let us define a co-ordinate $r$

$$r = -t \tag{43}$$

and the function $\tilde{q}_2(r)$ such that

$$\tilde{q}_2(r) = q_2(t) \tag{44}$$

Differentiating equation (41) with respect to $t$, using

$$\dot{q}_2(t) = \frac{dq_2(t)}{dt} = \frac{d\tilde{q}_2(r)}{dr}\frac{dr}{dt} = -\tilde{q}'(r) \tag{45}$$

using equations (41) and (44), and equating the result to equation (33), we obtain

$$\mathbf{\Phi} \begin{bmatrix} \dot{q}_1(t) \\ -\tilde{q}_2'(r) \end{bmatrix} = \mathbf{A}\mathbf{\Phi} \begin{bmatrix} q_1(t) \\ \tilde{q}_2(r) \end{bmatrix} + \mathbf{B}\, w_a(t) \tag{46}$$

Using

$$\mathbf{\Phi}^{-1}\mathbf{A}\mathbf{\Phi} = \begin{bmatrix} s_1 & 0 \\ 0 & s_2 \end{bmatrix} \tag{47}$$

we finally obtain

$$\dot{q}_1(t) = s_1 q_1(t) + b_1 w_a(t) \tag{48}$$

$$\tilde{q}_2'(r) = -s_2 q_2(r) - b_2 w_a(-r) \tag{49}$$

where $b_1$ and $b_2$ are

$$\mathbf{\Phi}^{-1}\mathbf{B} = \begin{bmatrix} b_1 \\ b_2 \end{bmatrix} \tag{50}$$

Using this time-reversal technique, we have obtained two stable differential equations for the system (equations (48) and (49)). (Note that $-s_2 = s_1$ is on the left half of the complex plane.) The first differential equation (equation (48)) runs forward in $t$, while the second one (equation (49)) runs backwards in $t$ or forward in $r$.

The boundary conditions require some consideration. Let us first analyze the case of finite-duration excitation in which

$$w(t) = 0 \quad t < t_0; \qquad w(t) = 0 \quad t > t_f \tag{51}$$

where $t_0$ and $t_f$ are times of beginning and end of the excitation signal. In this case, we can write $y(-\infty) = y(\infty) = 0$ and $\dot{y}(-\infty) = \dot{y}(\infty) = 0$, and the boundary conditions are specified as follows

$$q_1(-\infty) = 0, \qquad q_2(+\infty) = 0 \tag{52}$$

In the case of persistent constant excitation, such as

$$w(t) = w_0 U(t) \tag{53}$$

where $w_0$ is the constant magnitude of the signal and $U(t)$ the Heaviside function, we can write $y(-\infty) = \dot{y}(-\infty) = 0$, $y(\infty) = w_0/k$, and $\dot{y}(\infty) = 0$. The final value of $y(t)$ can be obtained from modal contributions as

$$y(\infty) = q_1(\infty) + q_2(\infty) = \frac{w_0}{k} \tag{54}$$

To compute $q_1(\infty)$ we note that $\lim_{t\to\infty} w_a(t) = w_0$ because the Hilbert transform of a constant signal is zero, and from equation (48) we obtain

$$\lim_{t\to\infty} q_1(t) = -\frac{b_1 w_0}{s_1} \tag{55}$$

Therefore, the boundary conditions should be specified as

$$q_1(-\infty) = 0, \qquad q_2(\infty) = w_0\left(\frac{1}{k} + \frac{b_1}{s_1}\right) \tag{56}$$

*4.3. Numerical integration of the differential equations*

For numerical implementation, we proceed as follows. Given a finite-duration excitation signal $w(t)$, the analytic signal $w_a(t)$ is constructed. Since the Hilbert transform is anticipatory and has memory, the analytic signal $w_a(t)$ starts before $w(t)$, and ends after $w(t)$ ends. Furthermore, since the response of the model anticipates the excitation, additional integration time has to be considered in the beginning and end tails. Therefore, an initial time $t_0$ and a final time $t_f$ can be defined such that $y_a(t)$ is arbitrarily small for $t < t_0$ and for $t > t_f$,

$$|y_a(t)| < \varepsilon, \quad t < t_0; \qquad |y_a(t)| < \varepsilon, \quad t > t_f \tag{57}$$

where $\varepsilon$ is a small positive number. Therefore, without significant loss of accuracy, the initial condition of the system can be taken as (see equation (52))

$$q_1(t_0) = 0, \qquad q_2(t_f) = 0 \tag{58}$$

To implement this solution numerically, we can use a zero-order hold on the sampled signal $w_a(t)$ and obtain a different equation for the system. Let the signal $w_a(t)$ be sampled with sampling time $\mathrm{d}T$. The generated sequence is

$$w_k = w_a(k\,\mathrm{d}T) \quad k = n_0, n_0 + 1, \ldots, n_f - 1, n_f \tag{59}$$

where $n_0$ is the integer closest to $t_0/\mathrm{d}T$, $n_f$ the integer closest to $t_f/\mathrm{d}T$, and $\mathrm{d}T$ the integration step.

Assuming $w_a(t)$ constant during the interval $[k\,\mathrm{d}T-(k+1)\,\mathrm{d}T]$ we can write

$$q_{k+1}^{(1)} = \mathrm{e}^{s_1\,\mathrm{d}T} q_k^{(1)} + (\mathrm{e}^{s_1\,\mathrm{d}T} - 1)\frac{b_1}{s_1} w_k, \qquad q_{n_0}^{(1)} = 0, \quad k = n_0, n_0 + 1, \ldots, n_f \tag{60}$$

$$q_{l-1}^{(2)} = \mathrm{e}^{-s_2\,\mathrm{d}T} q_l^{(2)} + (\mathrm{e}^{-s_2\,\mathrm{d}T} - 1)\frac{b_2}{s_2} w_l, \qquad q_{n_f}^{(2)} = 0, \quad l = n_f, n_f + 1, \ldots, n_0 \tag{61}$$

where $q_k^{(1)} = q_1(k\,\mathrm{d}T)$ and $q_l^{(2)} = q_2(l\,\mathrm{d}T)$ are the sampled analytic modal co-ordinates.

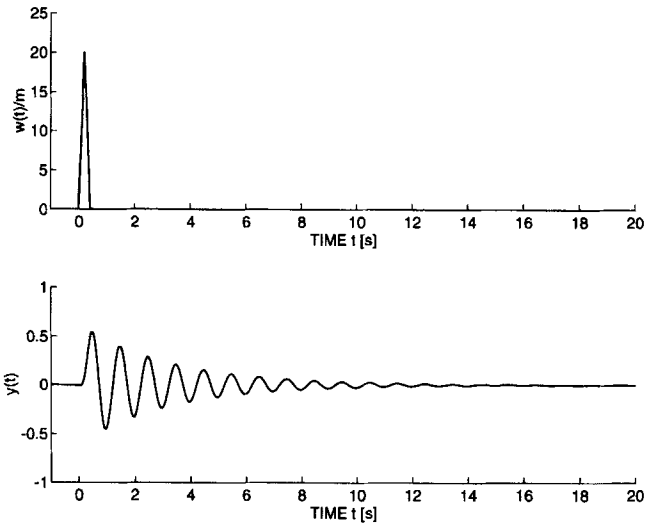


Figure 4. Response of a SDOF oscillator subjected to impulsive loading computed using the proposed technique

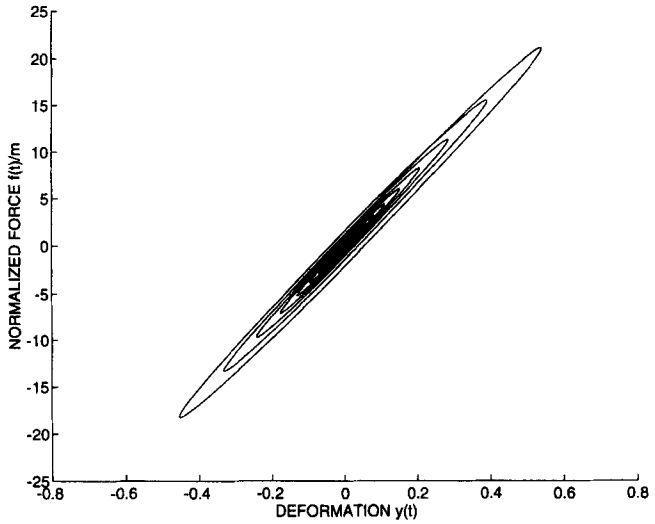


Figure 5. Hysteresis loops of a hysteretic Kelvin element ($\eta = 0{\cdot}10$)

Therefore, the numerical implementation involves the computation of the sampled sequence of the analytic signal $w_a(t)$, and step-by-step evaluation of equations (60) and (61). Finally, the response can be obtained as

$$\mathbf{x}_k = \mathrm{Re}\left[\boldsymbol{\Phi}\begin{bmatrix} q_k^{(1)} \\ q_k^{(2)} \end{bmatrix}\right], \qquad k = n_0, n_0 + 1, \ldots, n_f \tag{62}$$

where $\mathbf{x}^k = [y(k\,\mathrm{d}T)\ \dot{y}(k\,\mathrm{d}T)]^T$ is the sampled response of the oscillator described in equation (29).

Figure 4 shows in the top figure, an impulsive load applied to the SDOF oscillator described in equation (30). The response of the oscillator $y(t)$ computed using the proposed technique is shown in the bottom figure. The following oscillator parameters were assumed for the simulation: $\omega = 2\pi$ rad/s and $\eta = 0{\cdot}10$. The time step for the sampling time $\mathrm{d}T$ was 0·01 s. Figure 5 shows the computed normalized force in the hysteretic Kelvin element $f(t)/m = \mathrm{Re}[\omega^2 (1 + \mathrm{j}\eta)\, y_a(t)]$ as a function of the deformation $y(t)$.

*4.4. Extension to multi-degree-of-freedom structures*

The proposed technique can be utilized also in the case of multi-degree-of-freedom (MDOF) structures with linear hysteretic damping. Consider the following model of an $N$-degree-of-freedom structure

$$\mathbf{M}\ddot{\mathbf{y}}(t) + \mathbf{K}\mathbf{y}(t) + \mathbf{S}H[\mathbf{y}(t)] = \mathbf{L}_w\mathbf{w}(t) \tag{63}$$

where $\mathbf{M}$ is the positive-definite mass matrix, $\mathbf{K}$ the positive-definite stiffness matrix, $\mathbf{S}$ the hysteretic-damping matrix and $\mathbf{L}_w\,\mathbf{w}(t)$ the excitation vector.

Using analytic signals, this equation can be transformed into the following differential equation

$$\mathbf{M}\ddot{\mathbf{y}}_a(t) + (\mathbf{K} + j\mathbf{S})\mathbf{y}_a(t) = \mathbf{L}_w\mathbf{w}_a(t) \tag{64}$$

which can be expressed in state space as

$$\dot{\mathbf{x}}_a(t) = \mathbf{A}\mathbf{x}_a(t) + \mathbf{B}\mathbf{w}_a(t) \tag{65}$$

where

$$\mathbf{x}_a(t) = \begin{bmatrix} \mathbf{y}_a(t) \\ \dot{\mathbf{y}}_a(t) \end{bmatrix}, \qquad \mathbf{A} = \begin{bmatrix} \mathbf{O} & \mathbf{I} \\ -\mathbf{M}^{-1}(\mathbf{K} + j\mathbf{S}) & \mathbf{O} \end{bmatrix}, \qquad \mathbf{B} = \begin{bmatrix} \mathbf{O} \\ \mathbf{M}^{-1}\mathbf{L}_w \end{bmatrix} \tag{66}$$

and $\mathbf{y}_a(t)$, $\dot{\mathbf{y}}_a(t)$, and $\mathbf{w}_a(t)$ are analytic signals. As in the case of single-degree-of freedom structures with hysteretic Kelvin elements, the poles of this system show radial symmetry in the complex plane. Therefore, the integration of this set of differential equations can be carried out using the technique proposed. Using the eigenvectors of $\mathbf{A}$, the system can be uncoupled into $2N$ modal equations, and the differential equations of each of these modal co-ordinates can be integrated as shown previously. Those modal equations associated with stable poles are integrated forward in time, and those associated with unstable poles are integrated backwards in time.

Figure 6 shows a 2-DOF model of a structure used to illustrate the application of the technique to MDOF structures. The following parameters are assumed for the system

$$\mathbf{M} = m\mathbf{I}, \qquad \mathbf{K} = \begin{bmatrix} 200 & -100 \\ -100 & 100 \end{bmatrix} m(1/s^2), \qquad \mathbf{S} = \eta\mathbf{K} \tag{67}$$

The model is assumed to be classically damped (with a hysteretic damping matrix $\mathbf{S}$ proportional to the stiffness matrix $\mathbf{K}$). Figure 7 shows the poles of the system for $\eta$ in the range $0 < \eta < 1$. The poles of the system are shown with small circles in the figure, and solid lines are used to indicate the loss factor associated to the four poles of the system. In general, the poles of a structure with hysteretic damping appear in pairs with radial symmetry. However, in the case of a hysteretic-damping matrix proportional to the stiffness matrix, like the numerical example analyzed, all poles lie on a single line as can be observed in the figure.

Utilizing the proposed integration technique, the response of the model described in equation (67) to an impulsive excitation applied on the first degree of freedom was computed. The excitation signal is that shown in the top figure in Fig. 4. Figure 8 shows the computed response of the first degree of freedom of the model.

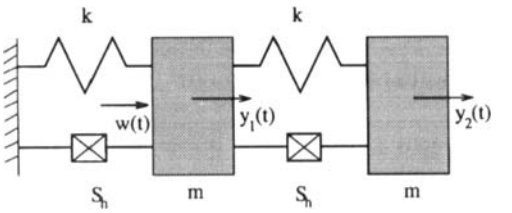


Figure 6. 2-DOF model used in the numerical example

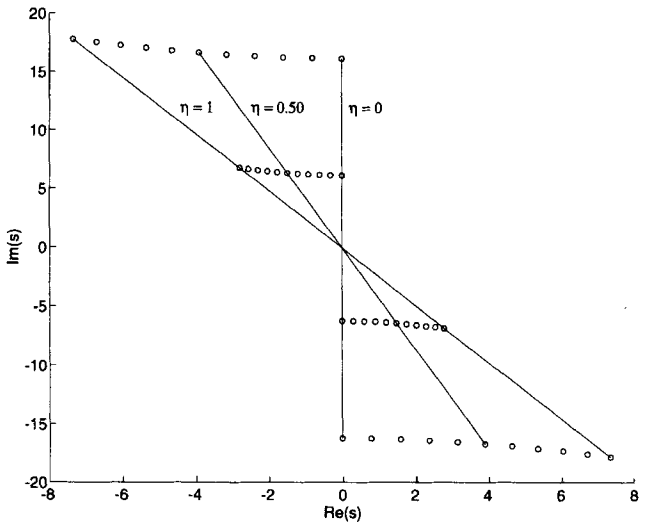


Figure 7. Poles of a 2-DOF structure with classical hysteretic damping for various values of the loss factor

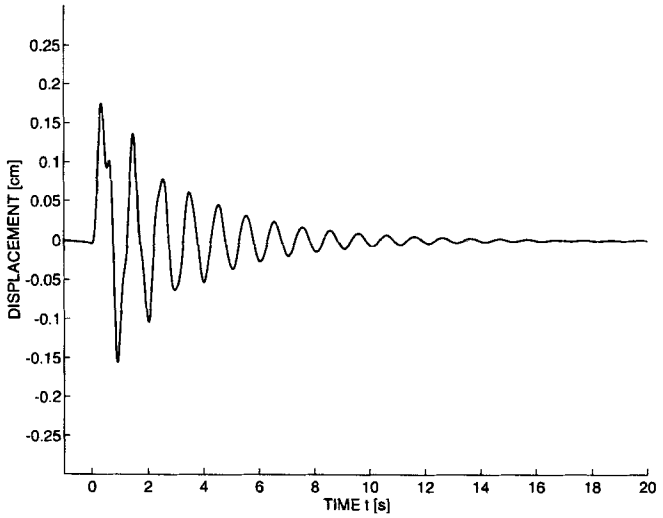


Figure 8. Response $y_1(t)$ of a 2-DOF structure with hysteretic damping subjected to impulsive loading computed using the proposed technique

## 5. HYSTERETIC MAXWELL ELEMENT

### *5.1. Hysteretic Maxwell element model using real-valued signals*

Many materials exhibit no resistance under sustained constant deformation and exhibit permanent deformation after load removal. The hysteretic Kelvin element cannot model this behaviour because of its finite static stiffness. Accordingly, another very similar model capable of modelling this behavior is presented in this section.

A linear hysteretic Maxwell element consists of a linear spring $k_0$ connected in series with a linear hysteretic damping element. The force in the spring is

$$f_s(t) = k_0 \Delta_s(t) \tag{68}$$

where $\Delta_s$ is the deformation of the spring and $k_0$ the spring constant. The force in the linear hysteretic damper can be expressed using the Hilbert transform as

$$f_d(t) = S_0 H[\Delta_d(t)] \tag{69}$$

where $\Delta_d(t)$ is the deformation of the hysteretic damper and $S_0$ the damper parameter. Since the spring and the damper are connected in series, the deformation of the element $\Delta(t)$ can be expressed as

$$\Delta(t) = \Delta_s(t) + \Delta_d(t) \tag{70}$$

From equations (69) and (70)

$$\Delta(t) = \frac{f_s(t)}{k_0} + \Delta_d(t) \tag{71}$$

Applying the Hilbert transform to equation (71) and using the fact that $f(t) = f_s(t) = f_d(t)$,

$$H[\Delta(t)] = \frac{H[f(t)]}{k_0} + H[\Delta_d(t)] \tag{72}$$

Finally, using equations (72) and (69), we obtain

$$\frac{H[f(t)]}{k_0} + \frac{f(t)}{S_0} = H[\Delta(t)] \tag{73}$$

which is the time-domain model of the hysteretic Maxwell element.

Let us compute the storage and loss moduli of this element. Applying Fourier transform to equation (73), we obtain

$$j\,\mathrm{sgn}(\bar{\omega})\Delta(j\bar{\omega}) = \frac{j\,\mathrm{sgn}(\bar{\omega})}{k_0} F(j\bar{\omega}) + \frac{F(j\bar{\omega})}{S_0} \tag{74}$$

and after some algebra,

$$F(j\bar{\omega}) = \left(\frac{S_0^2 k_0 |\mathrm{sgn}(\bar{\omega})|}{k_0^2 + S_0^2} + j\frac{k_0^2 S_0 \,\mathrm{sgn}(\bar{\omega})}{k_0^2 + S_0^2}\right)\Delta(j\bar{\omega}) \tag{75}$$

Comparing equations (24) and (75), we note that both the Kelvin and Maxwell models show constant storage and loss moduli for $\bar{\omega} \neq 0$. The only difference between the models is that in the Kelvin model, the storage modulus is non-zero at $\bar{\omega} = 0$, while in the Maxwell model it is zero at that frequency.

### *5.2. Hysteretic Maxwell model using analytic signals*

Differentiating equation (73) to eliminate all zero-frequency components, we obtain

$$H[\dot{\Delta}(t)] = \frac{H[\dot{f}(t)]}{k_0} + \frac{\dot{f}(t)}{S_h} \tag{76}$$

Applying the Hilbert transform to equation (76)

$$-\dot{\Delta}(t) = -\frac{\dot{f}(t)}{k_0} + \frac{H[\dot{f}(t)]}{S_h} \tag{77}$$

Summing equation (76) times $-j$ plus equation (77), we obtain, after simple algebra,

$$\dot{f}_a(t) = \beta \dot{\Delta}_a(t) \tag{78}$$

where $\dot{f}_a(t) = f(t) - jH[f(t)]$, $\dot{\Delta}_a(t) = \dot{\Delta}(t) - jH[\dot{\Delta}(t)]$, and

$$\beta = \frac{S_0^2 k_0 + jk_0^2 S_0}{S_0^2 + k_0^2} \tag{79}$$

Equation (79) is a consistent time-domain model for the hysteretic Maxwell model using analytic signals.

Consider a SDOF oscillator with a hysteretic Maxwell damping model whose equation of motion is

$$m\ddot{y}_a(t) + ky_a + f_a(t) = w_a(t)$$
$$\dot{f}_a(t) = \beta \dot{y}_a(t) \tag{80}$$

Defining $\omega = \sqrt{k/m}$, we can write

$$\dot{\mathbf{x}}_a(t) = \mathbf{A}\mathbf{x}_a(t) + \mathbf{B}w_a(t) \tag{81}$$

where

$$\mathbf{x}_a = \begin{bmatrix} y_a(t) \\ \dot{y}_a(t) \\ f_a(t) \end{bmatrix}, \quad \mathbf{A} = \begin{bmatrix} 0 & 1 & 0 \\ -\omega^2 & 0 & -1 \\ 0 & \dfrac{\beta}{m} & 0 \end{bmatrix}, \quad \mathbf{B} = \begin{bmatrix} 0 \\ \dfrac{1}{m} \\ 0 \end{bmatrix} \tag{82}$$

The solution of this differential equation can be obtained using the procedure utilized before. We can diagonalize the system of equations using the eigenvectors of **A**, and then integrate the differential equations of the modal co-ordinates forward in time for those with stable poles and backwards in time for those with unstable poles. Figure 9 illustrates an impulsive load and the corresponding response $y(t)$ of a SDOF oscillator with parameters $\omega = 2\pi$ rad/s, $S_0/m = 205{\cdot}3\ \text{l/s}^2$, and $k_0/m = 41{\cdot}06\ \text{l/s}^2$. For these parameters $\beta/m = 39{\cdot}48\ \text{l/s}^2 + \text{j}\ 7{\cdot}89\ \text{l/s}^2$. It can be shown that the response of this oscillator is the same as that of an SDOF oscillator in which the hysteretic Maxwell element is replaced by a hysteretic Kelvin element with appropriate parameters because the excitation signal considered is of finite duration and therefore, it does not contain a non-zero constant (zero-frequency component) (recall equations (24) and (75)). Hysteresis loops of a hysteretic Maxwell element are illustrated in Figure 10.

The parameters of equivalent Kelvin and Maxwell elements can be obtained by equating the storage and loss moduli of the hysteretic Maxwell element of that of the hysteretic Kelvin element for $\bar{\omega} \neq 0$,

$$\frac{S_0^2 k_0}{k_0^2 + S_0^2} = k \tag{83}$$

$$\frac{k_0^2 S_0}{k_0^2 + S_0^2} = S_h \tag{84}$$

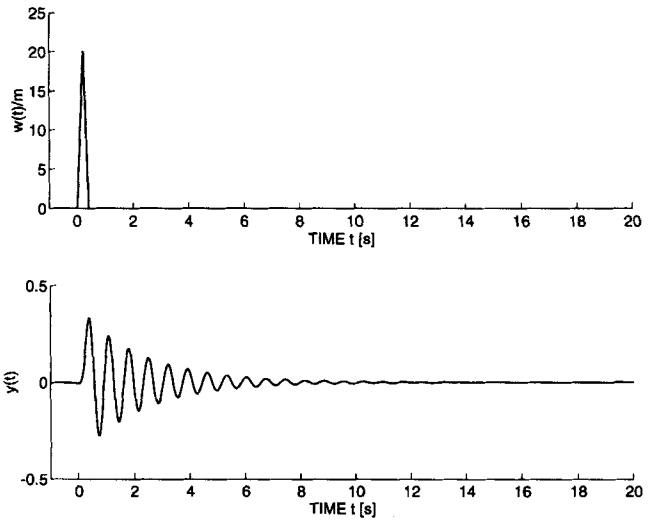


Figure 9. Response of a SDOF oscillator with hysteretic Maxwell damping subjected to impulsive loading computed with the proposed technique

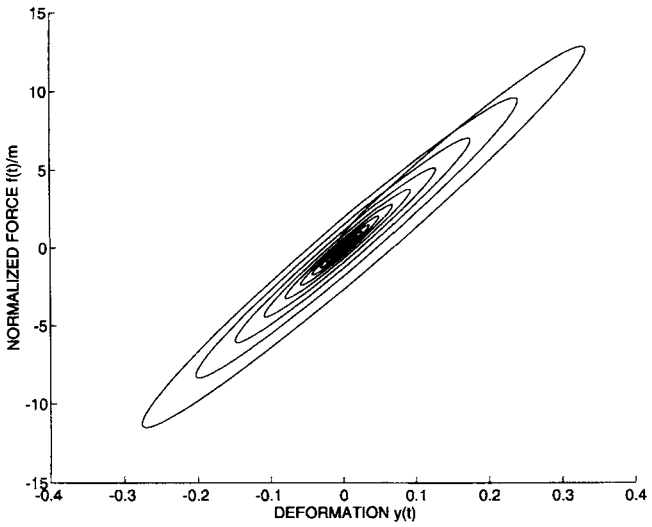


Figure 10. Hysteresis loops of a hysteretic Maxwell element

which gives the values of $k$ and $S_h$ that should be selected to obtain a Kelvin element that matches the Maxwell element with known parameters $k_0$ and $S_0$ for $\bar{\omega} \neq 0$. Solving for $k_0$ and $S_h$ as function of $S_h$ and $k$ we obtain the inverse relation

$$k_0 = \frac{S_h^2 + k^2}{k} \tag{85}$$

$$S_0 = \frac{S_h^2 + k^2}{S_h} \tag{86}$$

which gives the parameters of a Maxwell element as functions of those of a hysteretic Kelvin element.

## 6. CONCLUDING REMARKS

The concept of linear hysteretic damping has been addressed using time-domain methods. The hysteretic Maxwell element has been proposed as a model that shows no static resistance and identical forces to those of a hysteretic Kelvin element in the case of deformation signals without non-zero frequency components. It has been proven that using analytic signals, the integro–differential equations that model the response of structures with linear hysteretic damping can be transformed into ordinary differential equations. These equations, however, show unstable poles and therefore, require an integration technique by which the modal equations associated with unstable poles must be integrated backwards in time. For illustration purposes, the proposed technique was applied to the solution of simple numerical models that included hysteretic Kelvin and hysteretic Maxwell elements. The proposed integration scheme is an alternative to frequency-domain solutions that provides a time-domain analysis method significantly less costly than iterative techniques proposed in the literature.[17] These methods are valuable mainly in the context of linearization methods for a class of non-linear force–deformation relations that are being studied by the first author at present.[12, 13]

ACKNOWLEDGEMENTS

The authors would like to thank the reviewers for their valuable suggestions.

## APPENDIX

*Notation*

| | |
|---|---|
| $E[\Delta(t)]$ | operator on the deformation yielding the force in a mechanical element |
| $f(t)$ | real-valued force signal |
| $f_a(t)$ | analytic force signal |
| $G_s(\bar{\omega})$ | storage modulus |
| $G_l(\bar{\omega})$ | loss modulus |
| $H[y(t)]$ | Hilbert transform of a real-valued signal $y(t)$ |
| $\mathbf{I}$ | identity matrix |
| Im[ ] | imaginary part |
| j | imaginary unit ($\sqrt{-1}$) |
| $k, k_0$ | stiffness parameter |
| $\mathbf{P}$ | principal value of an integral |
| Re[ ] | real part |
| $s$ | complex number |
| $S_h, S_0$ | hysteretic-damping parameter |
| $U(t)$ | Heaviside function |
| $W_D$ | energy dissipation per cycle |
| $\hat{x}$ | Hilbert transform of $x(t)$ |
| $\dot{x}(t)$ | time derivative of $x(t)$ |
| $\Delta(t)$ | real-valued deformation signal |
| $\Delta_a(t)$ | analytic deformation signal |
| $\Delta_0$ | amplitude of a sinusoidal deformation signal |
| $\eta$ | loss factor |
| $\mathbf{\Phi}$ | matrix of eigenvectors |
| $\bar{\omega}$ | frequency variable in the Fourier transform of a signal |

## REFERENCES


1. M. A. Biot, 'Linear thermodynamics and the mechanics of solids', in *Proc. third U.S. national conf. applied mechanics*, American Society of Mechanical Engineers, New York, 1958, pp. 1–18.
2. T. K. Caughey, 'Vibration of dynamic systems with linear hysteretic damping (linear theory)', *Proc. fourth U.S. national congress of applied mechanics*, Vol. 1, American Society of Mechanical Engineers, New York, 1962, pp. 87–97.
3. C. G. Koh and J. M. Kelly, 'Application of fractional derivatives to seismic analysis of base isolated models', *Earthquake eng. struct. dyn.* **10**, 229–241 (1990).
4. N. Makris and M. C. Constantinou, 'Fractional-derivative Maxwell model for viscous dampers', *J. struct. eng. ASCE*, **117**, 2708–2724 (1991).
5. R. E. D. Bishop, 'The treatment of damping forces in vibration theory', *J. roy. aero. soc.* **59**, 738–742 (1955).
6. P. Lancaster, 'Free vibration and hysteretic damping', *J. roy. aero. soc.* **64**, 229 (1960).
7. S. H. Crandall, 'Dynamic response of systems with structural damping', in *Air, Space, and Instruments*, McGraw-Hill, New York, 1963.
8. Z. Liang and G. C. Lee, 'Damping of structures: Part 1-Theory of complex damping', *Report NCEER-91-0004*, National Center for Earthquake Engineering Research, Buffalo, New York, 1991.
9. N. Makris, 'The imaginary counterpart of recorded motions', *Earthquake eng. struct. dyn.* **23**, 265–273 (1994).
10. N. Makris, 'Constitutive models with complex parameters and the imaginary counter-part of records', *Proc. first world conf. on structural control*, Vol. 1, WP3/63-WP3/72, 1994.
11. T. K. Caughey and A. Vijayaraghavan, 'Free and forced oscillations of a dynamic system with linear hysteretic damping (non-linear theory)', *Int. j. non-linear mech.* **5**, 533–555 (1970).
12. J. A. Inaudi, D. K. Nims and J. M. Kelly, 'On the analysis of structures with energy dissipating restraints', *EERC Report No. 93/13*, Earthquake Engineering Research Center, University of California at Berkeley, 1993.
13. J. A. Inaudi, J. Hayen and W. Iwan, 'Semi-active damping brace system', *J. eng. mech.*, ASCE. (submitted for publication).
14. J. A. Inaudi and J. M. Kelly, 'A friction mass damper for vibration control', *Report No. UCB/EERC-92/18*, Earthquake Engineering Research Center, University of California at Berkeley, 1992.
15. D. C. Champeney, *A Handbook of Fourier Theorems*, Cambridge University Press, Cambridge, 1987.
16. R. N. Bracewell, *The Fourier transform and its applications*, McGraw-Hill, New York, 1986.

17. J. A. Inaudi and J. M. Kelly, 'Linear hysteretic damping and the Hilbert transform', *J. eng. mech.*, ASCE **121**, 636–632 (1995).
18. J. A. Inaudi, A. Zambrano and J. M. Kelly, 'On the analysis of linear structures with viscoelastic dampers', *Report No. UCB/EERC/93-09*, Earthquake Engineering Research Center, University of California at Berkeley, 1993.
19. J. Argyris and H. P. Mlejnek, *Dynamics of Structures*, Text on Computational Mechanics, Volume V, North-Holland, Amsterdam, 1991.
20. R. W. Clough and J. Penzien, *Dynamics of Structures*, 2nd edn, McGraw-Hill, New York, 1993.
21. A. K. Chopra, *Dynamics of Structures: Theory and Applications to Earthquake Engineering*, Prentice Hall, Englewood Cliffs, NJ, 1995.